On the attitude stability of flying dandelion seeds

Lang Qin (秦琅) ; Zhen Jian (菅振) ; Yeyin Xu (徐业银) ; Lifeng Ma (马利锋)

Check for updates

View Online

Export Citation

CrossMark

Articles You May Be Interested In

Completing the dark matter solutions in degenerate Kaluza-Klein theory

J. Math. Phys. (April 2019)

Gibbs measures based on 1d (an)harmonic oscillators as mean-field limits

J. Math. Phys. (April 2018)

An upper diameter bound for compact Ricci solitons with application to the Hitchin–Thorpe inequality. II

J. Math. Phys. (April 2018)

Physics of Fluids

AIP Publishing

On the attitude stability of flying dandelion seeds 🅕 🆂🅲🅸

View Online　　Export Citation　　CrossMark

Lang Qin (秦琅),[1] 🆔 Zhen Jian (菅振),[1,2,a] 🆔 Yeyin Xu (徐业银),[1] 🆔 and Lifeng Ma (马利锋)[1,3,a] 🆔

AFFILIATIONS

[1]State Key Laboratory for Strength and Vibration of Mechanical Structures, Department of Engineering Mechanics,
School of Aerospace Engineering, Xi'an Jiaotong University, Xi'an 710049, China
[2]Research Institute of Xi'an Jiaotong University, Zhejiang, Hangzhou 311215, China
[3]Department of Mechanical, Materials and Manufacturing Engineering, the University of Nottingham, University Park NG7 2RD,
United Kingdom

[a]Authors to whom correspondence should be addressed: zhenjian@xjtu.edu.cn and malf@mail.xjtu.edu.cn

ABSTRACT

Dandelion seeds possess a complex three-dimensional structure and a self-adapted flying ability. To understand this fascinating flight mechanism, a three-dimensional umbrella-shaped model imitating dandelion seeds is proposed. The effects of folding angle and flow velocity on the dandelion drag force during their descent are studied, and it is found that the larger folding angle results in a smaller drag coefficient. Four different vortex structures are revealed depending on the folding angle. The effect of crosswind disturbances on the attitude stability of dandelions is also investigated by changing folding angles. It is found that dandelions with larger folding angles have better attitude stability. The proposed model suggests that when the folding angle is between 20° and 40°, the dandelion seeds might have a good balance between the drag force and attitude stability, which ensures a broad self-adapted flying ability.

Published under an exclusive license by AIP Publishing. https://doi.org/10.1063/5.0160735

I. INTRODUCTION

Many flowering plants have unique methods of seed dispersal.[1,2] For example, certain species, such as poplars, willows, and dandelion seeds, effectively utilize passive wind dispersal mechanisms to propagate their seeds. This mechanism has inspired the development of efficient non-powered vehicles.[3,4] Dandelion seeds exhibit a unique morphology, characterized by approximately one hundred radiating filamentous structures extending from the pappus.[5–7] This morphology leads to a high drag coefficient, resulting in prolonged floating periods in the air. Owing to their high drag coefficient and stability during flight, dandelion seeds are capable of traveling distances up to 30 km.[8–10]

A number of experiments indicate that the drag coefficient of the dandelion is much higher than that of dense structures with the same projected area, and the folding angle of the dandelion has a definite effect on its drag force. By using particle image velocimetry technology (PIV), Cummins et al.[11] investigated the flow structure of the dandelion in the vertical upward wind. They found a pair of stable vortex rings separated from the upper side of the dandelion. They referred to this vortex as the separated vortex ring (SVR), which helps to maintain a stable flight of the dandelion seeds. They also found that the air drag force of dandelion seeds is much higher than that of a solid disk structure. Zussman et al.[12] measured the terminal velocity and drag coefficient of some pyramid-

shaped nonwoven pads made of nanofibers with sub-micrometer diameters using the free fall method. The results showed that the drag coefficient of porous membrane structures is much higher than impermeable membrane structures. Meng et al.[13] and Seale et al.[14,15] investigated the correlation between humidity and the folding angle of the dandelion. The results showed that air humidity has a significant influence on the folding angle of dandelion seeds, which affects their drag coefficient and drift distance. These experiments show that the special structural parameters of the dandelion, especially the folding angle, have a large effect on the drag force, but the folding angle on the drag force and attitude stability of dandelion seeds still needs a thorough analysis.

Apart from experimental studies, a great deal of numerical simulations have been carried out in the literature. The structure of the dandelion is often simplified into a flat plane consisting of a central disk with filaments radially distributed around it. This plane has the same porosity as the dandelion. Qiu et al.[16,17] studied the effect of porosity on the separation vortex ring (SVR) and found that when the flow direction and the axial direction of the dandelion are misaligned, a horizontal force and a recovery moment opposite to the deflection direction are generated at the lower side of the dandelion. Qiu et al.[18] also pointed out that the pappus angle is the key factor that affects the complete separation of SVR from dandelion seed pappus. Dong

et al.[19] and Li *et al.*[20] simplified the dandelion filaments as rectangular prisms and investigated the effects of porosity and prism width on the dandelion vortex structure and drag force. Casseau *et al.*[21] simplified Tragopogon pratensis into a parachute model with permeability. They found that the permeability of the parachute can divide the wake flow into three states and that the wake flow state can also affect the stability and drag coefficient of the parachute. Some three-dimensional structural features of dandelion, such as the folding angle of filament, are neglected by the plane disk simplified model of dandelion. The drag force and the SVR of the dandelion may be affected by these features, so that the models which better match the three-dimensional structural features of the dandelion seeds need to be further developed.

The vortex stability of dandelion seeds has been an intriguing research point. In a uniform flow field, the wake of porous objects can also form stable vortex structures. Ciuti *et al.*[22] studied the wake morphology and stability characteristics of porous spheres and observed that within a certain range of porosity, the vortices penetrated into the interior of the spheres, reducing the threshold Reynolds number for flow instability. The wake structure of porous disks was found to be greatly influenced by the Darcy number. Above a critical Darcy number ($Da > 10^{-3}$), the recirculation region could not be maintained.[23,24] The aspect ratio (the ratio of length to thickness of the structure) also is an important indicator of vortex structure. For low porosity, high aspect ratio disks produce larger wakes, while for high porosity, the opposite trend is observed.[25] Researchers have also experimentally studied the structure of cylindrical arrays,[26] honeycomb disks,[27] and porous cylinders[28] to investigate the effect of porosity on wake stability and drag force under different structures. Ledda *et al.*[29,30] used a linear stability theory-based method to determine the average porosity threshold for stable symmetric vortices in the flow field. Fabre *et al.*[31] discussed the stability of a two-dimensional disk in free fall motion driven by gravity. Tchoufag *et al.*[32] investigated the stability of ascending or descending paths driven by gravity or buoyancy under different aspect ratio disks. These porous media approximate structures, and theoretical studies are mainly focused on discussing the stability of wake vortex structures. However, the flight stability analysis of dense disk-like structures may not be applicable to dandelion structures with higher porosity. Thus, more efforts are needed for the flight stability analysis of dandelion seeds during flight.

In this study, a geometric model is established according to the structural properties of dandelion seeds with a variable folding angle. Based on this model, we aim to: (i) explore the effect of the dandelion folding angle on the dandelion wake vortex structure and the air resistance of dandelion and (ii) study the effect of the folding angle on its attitude stability. It is expected that this study may shed some light on the design of dandelion-like aircraft.

The paper is structured as follows: Sec. II outlines the numerical setup, including the geometric model simplification, turbulence model, and grid scheme. Section III explores the vortex ring structure, drag coefficient, and attitude stability. Finally, Sec. IV presents the conclusions.

II. NUMERICAL SETUP
A. Dandelion umbrella model

Dandelion seeds were gathered at the campus of Xi'an Jiaotong University, with the photograph displayed in Fig. 1(a). As demonstrated in Fig. 1(a), the filaments of the dandelion naturally assemble themselves in a form of an inverted umbrella. Based on this angular characteristic, we propose a dandelion umbrella model shown in Figs. 1(b) and 1(c) (side view and top view). Figure 1(d) gives various characteristic parameters of the geometric structure of the dandelion umbrella model.

We define the angle between the filament and the *r*-axis as α, which is the folding angle of the dandelion. In nature, the folding angle α typically ranges from 4° to 54°.[13] In our model, we chose a larger range of the folding angles from 0° to 60°. As shown in Fig. 1(c) (top view), the dandelion model consists of 80 filaments ($n_f = 80$) spaced evenly with an equal interval of 4.5°. Each filament is a slender cylinder with a diameter of $d_f = 0.02$ mm and a length of $l = 5.5$ mm. The base diameter of the model is $d_p = 0.65$ mm, and the base thickness is $t_p = 0.04$ mm. Then, the projection diameter of the model along the *r*-axis is $D = d_p + 2l \cos \alpha$. The porosity of a dandelion is defined as the ratio of the projected area of the void to the area of the circle whose radius is given by the most extended filament. The schematic diagram of the dandelion projection in Fig. 2(a) allows us to
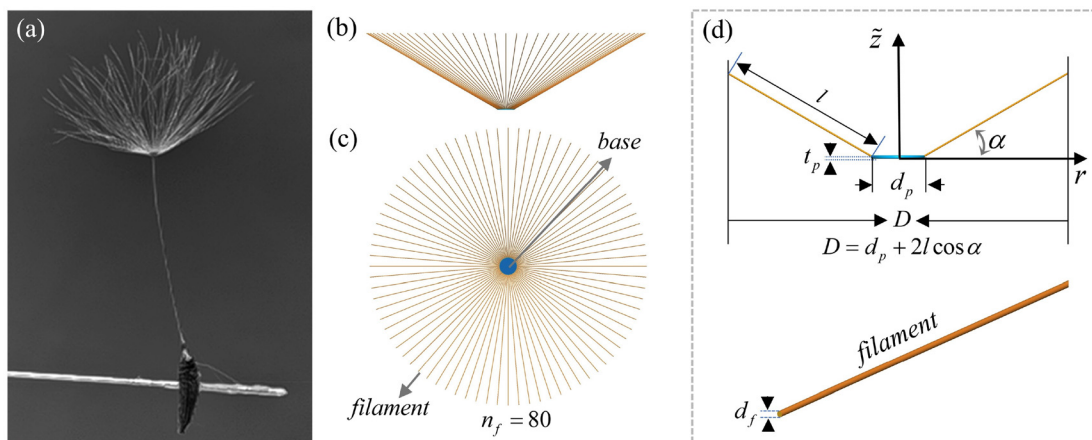

FIG. 1. (a) Photograph of dandelion seed, (b) side view of the dandelion model, (c) top view, and (d) the geometry of the model.
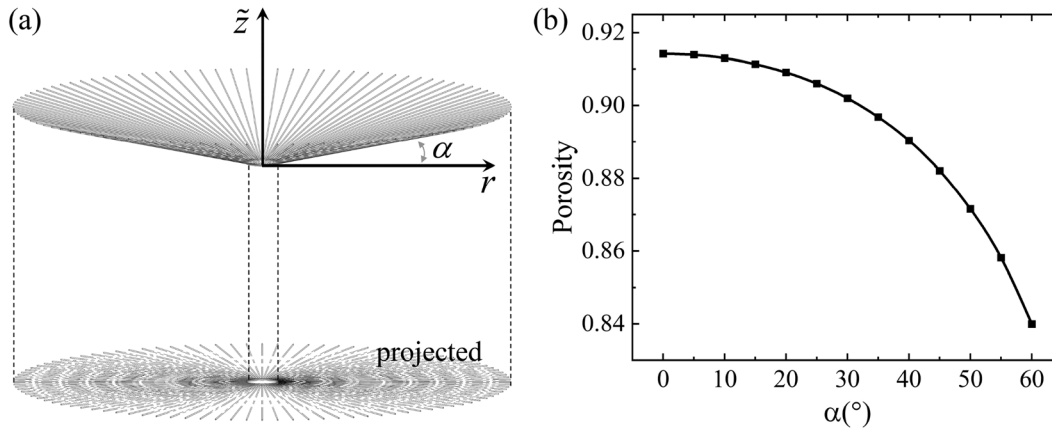
FIG. 2. (a) The dandelion projected along the z axis and (b) porosity curve varies with α.

derive the equation that describes the relationship between the dandelion porosity and the folding angle α as follows:

$$\phi = 1 - \frac{n_f d_f l \cos \alpha + \pi (d_p/2)^2}{\pi (l \cos \alpha + d_p/2)}, \quad (0° \leqslant \alpha \leqslant 60°), \quad (1)$$

the formula for calculating the projected area of the dandelion umbrella-shaped model is as follows:

$$A = n_f d_f l \cos \alpha + \pi (d_p/2)^2. \quad (2)$$

In nature, the porosity of dandelion is approximately 0.916.[11] As shown in Fig. 2(b), the porosity decreases with the increase in the folding angle $\alpha (0 \leq \alpha \leq 60°)$. At $\alpha = 0°$, the porosity attains the maximum value of 0.915, while at $\alpha = 60°$, the porosity reaches the minimum value of 0.84.

The air drag force F_D acting on the dandelion model is directly proportional to its projected surface area A. Subsequently, after

calculating the air resistance of dandelions, we can rapidly calculate the drag coefficient of dandelions C_D under different folding angles α as the following formula:

$$C_D = \frac{F_D}{0.5 \rho U^2 A}, \quad (3)$$

where ρ is the density of air, and U is the inflow velocity of the airflow.

B. Numerical simulation methods

The continuity equation for incompressible flow can be expressed as

$$\nabla \cdot \boldsymbol{u} = 0, \quad (4)$$

where $\boldsymbol{u}$ denotes the velocity vector. Furthermore, the Navier–Stokes equations are utilized to simulate the motion of the fluid. For incompressible flow with no external forces, the Navier–Stokes equations are simplified to
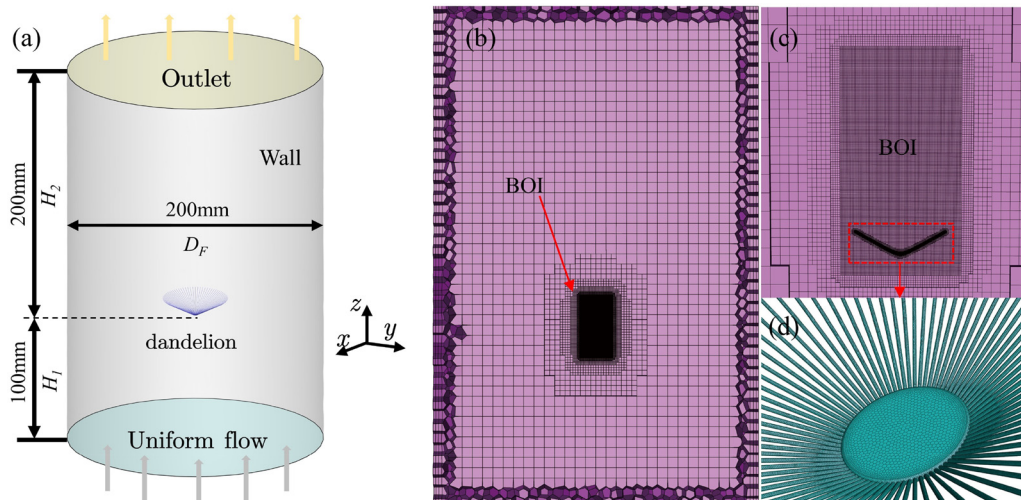

FIG. 3. (a) Computational domain and boundary conditions, (b) the grid of the fluid domain and the BOI, (c) zoomed-in view of grid of BOI zone, and (d) zoomed view of girds of the dandelion.

TABLE I. Different grid configurations and the number of grids.

Mesh	Mesh-1	Mesh-2	Mesh-3	Mesh-4
Boundary layer number (B)	6	7	8	9
Minimum cell size (mm)	0.008	0.006	0.005	0.004
Total grids	8 399 544	12 927 954	14 396 856	17 695 241
Maximum error (ε)	4.86%	2.268%	0.503%	0

$$\rho(\partial\boldsymbol{u}/\partial t + \boldsymbol{u}\cdot\nabla\boldsymbol{u}) = -\nabla p + \mu\nabla^2\boldsymbol{u}, \tag{5}$$

where ρ is the fluid density, t is the time, p is the pressure, μ is the fluid's dynamic viscosity, and $\nabla^2\boldsymbol{u}$ is the Laplacian of the velocity field. With appropriate boundary conditions, this equation can be solved to obtain the velocity field of the fluid surrounding the dandelion.

The laminar model is used to simulate the steady-state flow in this study. The numerical algorithm is based on the coupled methodology with the Rhie–Chow interpolation scheme to prevent the decoupling of velocity and pressure fields. As shown in Fig. 3(a), the computational domain is modeled as a cylinder, and the dandelion seed is vertically fixed on its central axis. The dandelion is proportionally enlarged to show its position in the fluid domain. The distance between the dandelion and the inlet is denoted by H_1, and the distance between the dandelion and the outlet is represented by H_2. The diameter of the domain is 200 mm. When $\alpha = 0°$, the dandelion achieves its maximum diameter $D_{\max} = d_p + 2l = 11.65$ mm. $H_1 = D_F/2 > 8D_{\max}$, which meets the calculation requirements. In this simulation, the dandelion model structure is assumed to be rigid. For computational efficiency, Boolean operations are utilized to eliminate the solid dandelion model from the fluid domain, thereby leaving only the fluid region. Furthermore, the dandelion's exterior surface is set up as a wall boundary. As shown in Fig. 3(b), in order to provide a better grid configuration, we use the Mosaic Poly-Hexcore grid, which is a combination of polyhedron surface grid and hexahedral internal core grid. To enhance the accuracy of the simulation, a body of influence (BOI) encroachment zone is employed around the dandelion. The

BOI zone is a cylindrical region that can effectively encompass the primary vortex structure [see Fig. 3(c)]. Figure 3(d) shows the polyhedral mesh of the surface of the dandelion.

To verify the grid independence, four grid configurations were set up. The detailed information of four sets of meshes is summarized in Table I. Multiple boundary layers were added to the dandelion surface. The minimum cell size is located on and near the surface of the dandelion. The most refined mesh, Mesh-4, is utilized as a benchmark to evaluate the computational error, denoted as $\varepsilon = (P_i - P_4)/P_4 \times 100\%$. The maximum error for each mesh size is cataloged in Table I.

Figure 4 shows the pressure distribution contour on the $z - y$ plane and the dandelion surface. To perform the grid independence verification, we introduced a line segment c positioned along the z-axis, starting from the origin o. The length of the line segment is equal to the projected length D of the dandelion model. It can be observed from Fig. 4 that under a stable flow field, the pressure distribution exhibits a symmetrical configuration. Evidently, the axis of symmetry in this pressure distribution aligns rightly with that of the dandelion model.

Figure 5 displays the pressure distribution around and within the dandelion. As can be seen from the inset image, the upper side of the dandelion shows a low-pressure distribution, while the lower side has a high-pressure distribution.

Due to the complex structure of the dandelion, the precise control over the dimensionless distance $y+$ is required to setup the grid.
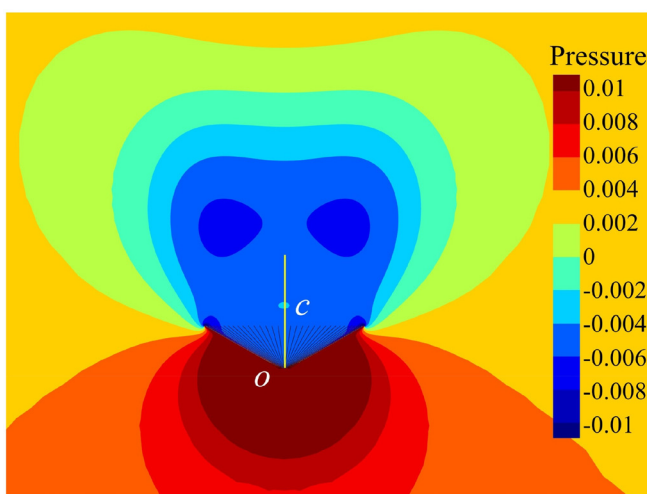

FIG. 4. Pressure contour in the z–y plane at $\alpha = 30°$ and $U = 0.2$ m/s.
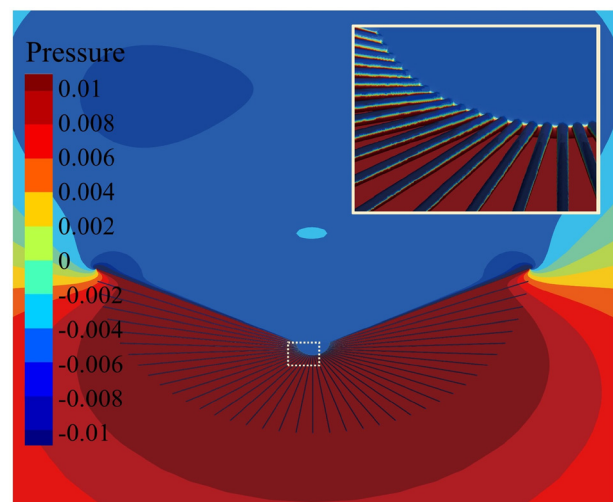

FIG. 5. The pressure distribution on the surface of the dandelion model and its vicinity.

In this study, we established the height of the first layer of the grid to be 0.008 mm, with a growth rate of 1.2, while maintaining a maximum aspect ratio of 14.03. This configuration ensures that the $y+$ values are less than 1 in all numerical scenarios. This design not only ensures the accuracy of the simulation but also meets the requirements for grid independence. The grid independence verification is performed based on the pressure distribution on the line segment c under different grid configurations. As shown in Fig. 6, the pressure distribution along the line segment c in the Mesh-3 configuration is remarkably close to their counterparts in the Mesh-4 configuration, and they almost complete overlap. The maximum error between them is less than 0.503%, satisfying the prescribed computational accuracy. Hence, Mesh-3 was employed for subsequent computations.

The uniform velocity boundary condition is imposed at the inlet, and the pressure outlet boundary condition is imposed at the outlet. The inlet uniform velocity is larger than zero. Both the surface of the dandelion and the cylindrical boundary are set as non-slip surfaces. Air is set as an incompressible ideal gas, with the air density of $\rho = 1.204 \, \text{kg/m}^3$ and the viscosity constant of $\mu = 1.511 \times 10^{-7} \, \text{m}^2/\text{s}$. The Reynolds number is defined as

$$\text{Re} = \frac{\rho U D}{\mu}, \tag{6}$$

where D is the dandelion projected diameter, and U is the incoming flow velocity.

Figure 7 illustrates the variation curves of the Reynolds number and dandelion folding angle at different speeds. It can be seen that Reynolds number decreases gradually as the folding angle gradually increases. This is because as the folding angle gradually increases, the characteristic length $D = d_p + 2l \cos \alpha$ gradually decreases. To investigate the effect of the folding angle on the flow field at different flow velocities, the incoming flow velocity U and the folding angle α are regarded as the main variables. In this study, the incoming flow velocity is $U \leq 0.8$ m/s, with the corresponding $\text{Re} \leq 620$.
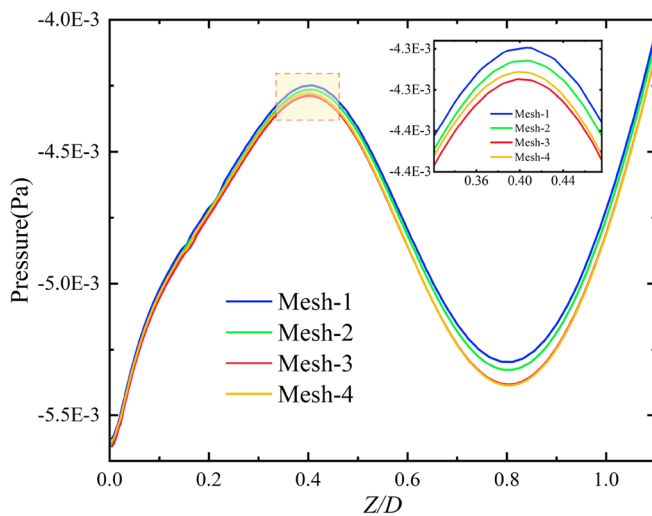

FIG. 6. The pressure distribution along line segment c in Fig. 4 for different grid configurations.
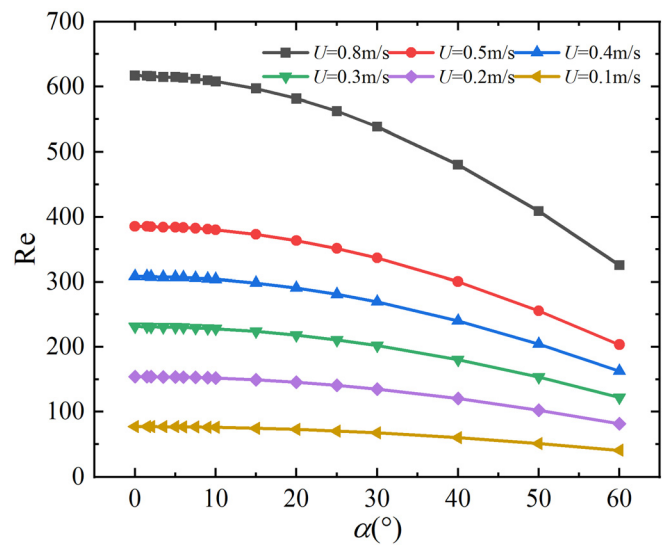

FIG. 7. The relationship between the Reynolds number and the folding angle of the dandelion under different velocities.

III. RESULTS AND DISCUSSION

We will focus on two aspects in the following: (i) the influence of the folding angle of the dandelion on its vortex structure and air drag force and (ii) the attitude stability of the dandelion under a deflection angle between its axial direction and the flow direction.

A. Effect of folding angle on vortex structure and drag force

The critical point theory posits that, in the case where a matrix $A_{ij} = \partial u_i / \partial x_j$ exists with one real eigenvalue and a pair of complex conjugate eigenvalues, the fluid flow is characterized as helical-saddle shaped.[33] Using the critical point theory, we can quickly find the center of the vortex. In the three-dimensional vortex structure, the center of the vortex forms a vortex core circle (VCC) [see Fig. 8(a)]. Under certain computational conditions, we found two VCCs in the flow field of the dandelion. The large vortex and the small vortex corresponding to these two VCCs are defined as the primary vortex and secondary vortex, respectively [see Fig. 8(b)].

Based on the existence of the secondary vortex and the position of the downstream stagnation point of the primary vortex, the vortex structure can be classified into the following four types in terms of the folding angle and inflow velocity:

I. There is no secondary vortex, and the downstream stagnation point is located at the origin point ($z_{su} = 0$). The primary vortex still attaches to the dandelion [Fig. 9(a)].

II. The secondary vortex exists, and the downstream stagnation point is located at the origin point ($z_{su} = 0$). The primary vortex still attaches to the dandelion [Fig. 9(b)].

III. The secondary vortex exists, and the downstream stagnation point is located above the origin point ($z_{su} > 0$). At this point, the primary vortex and the secondary vortex share a
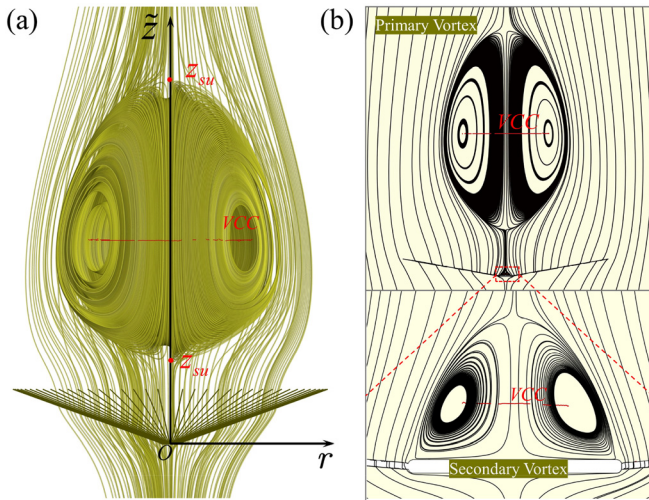
FIG. 8. (a) Definitions of various parameters of dandelion vortex structure and (b) the primary vortex and the secondary vortex.

FIG. 10. Vortex structure phase diagram.

saddle point. The primary vortex still attaches to the dandelion [Fig. 9(c)].

IV. There is no secondary vortex, and the downstream point z_{su} of the primary vortex moves further upward ($z_{su} > 0$), causing a more obvious separation between the primary vortex and the dandelion [Fig. 9(d)].

After a series of simulations, a phase diagram is plotted to show the variation of vortex structure patterns by changing the folding angle α and the inflow velocity (see Fig. 10). The region corresponding to type II is relatively narrow, indicating that pattern II is unstable and

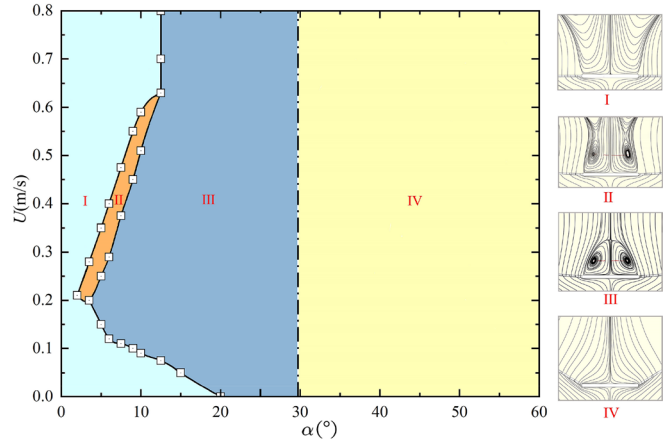quickly transitions into patterns I or III under perturbations. When α is greater than 29°, only type IV is observed.

As shown in Fig. 11(a), at the same folding angle, the drag coefficient of the dandelion gradually decreases with increasing velocity. Figure 11(b) depicts that at the same velocity, the air drag coefficient gradually decreases with increasing folding angle α. This implies that, in Fig. 10, the drag coefficient decreases with the increase in the folding angle and the incoming flow velocity, seemingly regardless of the flow patterns.

B. Effect of folding angle on attitude stability

During dandelion's falling, it may experience disturbances from crosswinds, so that the dandelion's flow field is analyzed with the co-
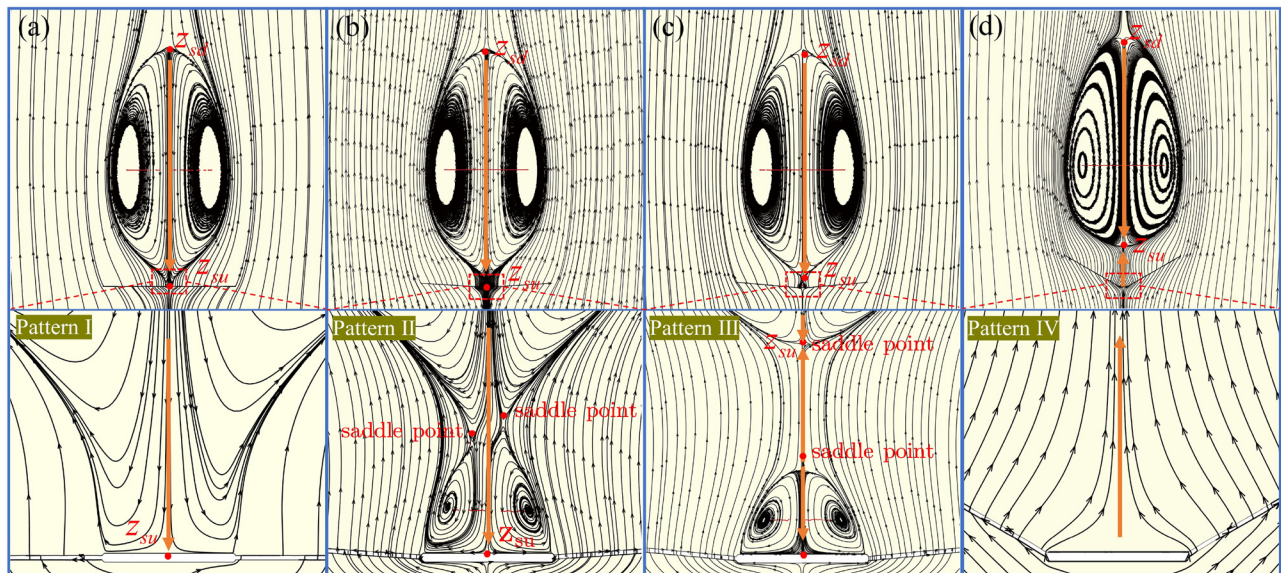

FIG. 9. The primary vortex and the secondary vortex (a) pattern I, (b) pattern II, (c) pattern III, and (d) pattern IV.
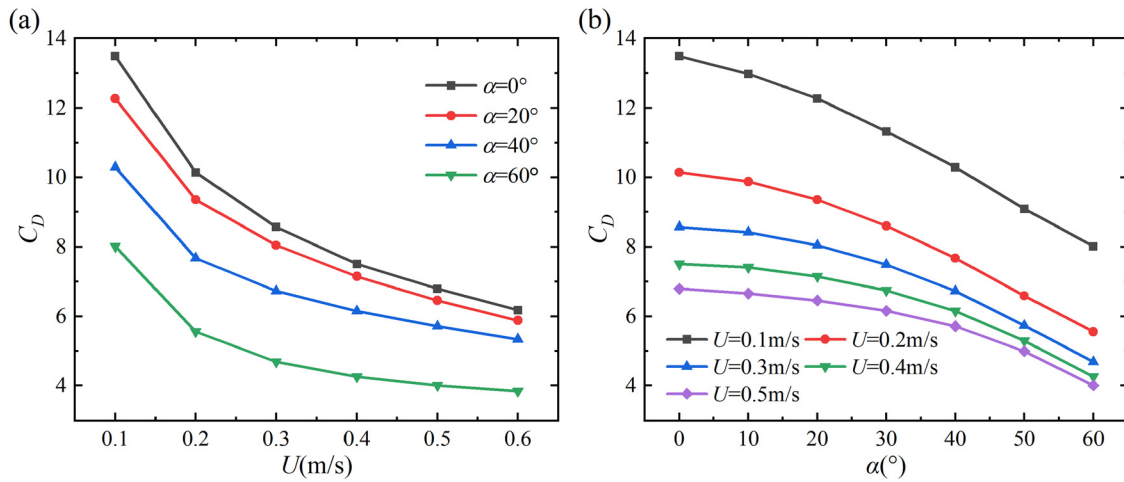
FIG. 11. (a) Drag coefficient varying with velocity and (b) drag coefficient varying with the folding angle.
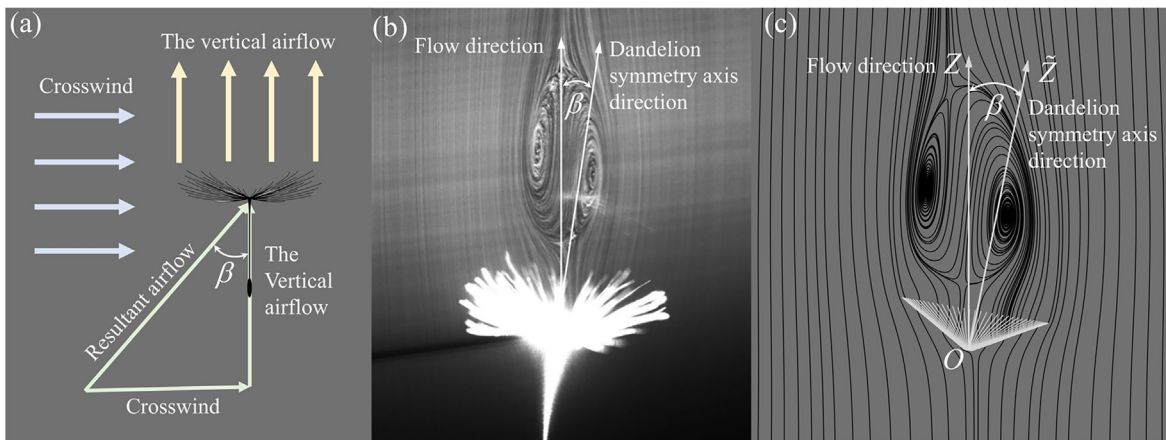

FIG. 12. (a) Schematic diagram of the resultant wind from lateral and vertical directions, (b) PIV images of dandelion flow field under deflection angle (reproduced with permission from Cathal Cummins *et al.*, Nature **562**, 7727 (2018). Copyright 2018 Spring Nature.), and (c) the simulated dandelion flow field under deflection angle.

action of crosswind and vertical winds in this study. The resultant of the crosswind and vertical wind is presented in Fig. 12(a). The intensity of the crosswind is characterized by the angle between the resultant and vertical winds, which is termed as the incoming flow angle, β.

This angle also represents the difference between the dandelion's axially symmetric direction and the resultant wind direction. Figure 12(b) depicts the actual particle image velocimetry (PIV) flow field of the dandelion when $\beta > 0°$, where the symmetry of the vortex structure is disrupted.

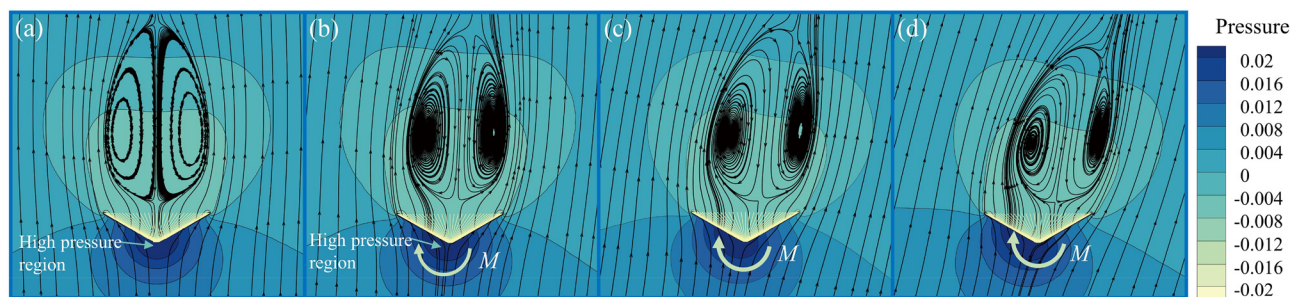**FIG. 13.** Pressure distribution and streamline with a flow velocity of 0.2 m/s at different deflection angles: (a) $\beta = 0°$, (b) $\beta = 5°$, (c) $\beta = 10°$, and (d) $\beta = 15°$.
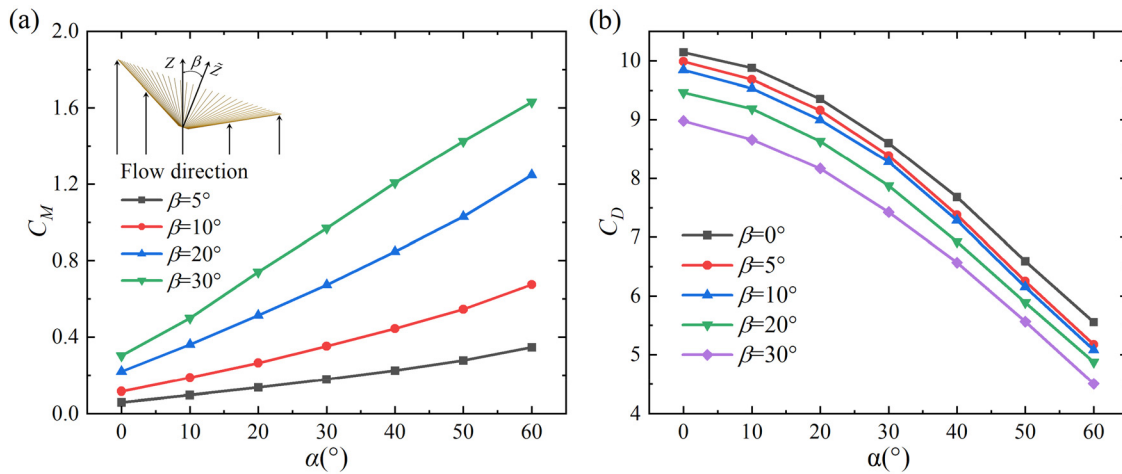
FIG. 14. At $U = 0.2$ m/s, (a) curve of the restoring moment coefficient of the dandelion with α and (b) the variation curve of the drag coefficient of the cattail with α.

Figure 12(c) illustrates the streamline of the dandelion model, simulated at $\beta > 0°$. Both Figs. 12(b) and 12(c) are obtained with an incoming flow velocity $U = 0.391$ m/s. By comparing Fig. 12(b) with Fig. 12(c), it can be found that the vortex structure of the simulation results is quite similar to the vortex structure in the PIV image.

Figure 13 displays the evolution of the dandelion flow field's pressure distribution and streamline patterns as the incoming flow angle, β, sequentially increases from 0° to 15°. In the absence of a crosswind ($\beta = 0°$), both the dandelion's primary vortex structure and the pressure distribution within the flow field exhibit symmetrical patterns. Yet, with an increasing intensity of the crosswind (reflected by a rising incoming flow angle β), the symmetry of both the vortex structure and pressure distribution becomes disrupted. The high-pressure region beneath the dandelion starts shifting left, creating a restorative, clockwise torque around the dandelion's base. This torque induces a rightward drift of the dandelion, and when its symmetry axis aligns parallelly with the flow, the symmetry of the vortex structure and pressure distribution is restored. These results reflect the dandelion's outstanding capability for self-adjusting attitude stability.

The moment coefficient C_M is defined as

$$C_M = \frac{M}{0.5\rho U^2 A},\qquad(7)$$

which can facilitate a more comprehensive examination of the influence of angles α and β on the recovery moment. Figure 14(a) presents the variations of the moment coefficients with angles of α and β respectively. At a constant α angle, the restoring moment coefficient increases as β increases. This can be intuitively understood as the greater deviation of the tumbler from its equilibrium position, the larger force that acts to restore it. At a constant α angle, the coefficient of restoring torque increases with increasing β, which reveals that the larger deflection, the stronger its restoring force. Under the same β angle, the coefficient of restoring torque also increases with increasing α, indicating that models with larger α angles have better restorative ability. Figure 14(b) shows that in the absence of crosswind interference ($\beta = 0°$), the dandelion reaches its maximum air drag force when its folding angle α is zero, which enables it to remain airborne

for a prolonged duration. However, to achieve long-distance flight, it must utilize the power of crosswinds. In this scenario, an appropriate folding angle is indispensable, as it enhances the attitude stability of the dandelion. Therefore, a dandelion seed with a proper folding angle α can maintain a high drag coefficient and good attitude stability, which is also consistent with the natural selection of the dandelion. Our model demonstrates that when the folding angle is approximately between 20° and 40°, it not only has good attitude stability but also has a large drag force.

IV. CONCLUSION

In this paper, a 3D dandelion umbrella model with an adjustable folding angle has been proposed to investigate the influence of the folding angle of the dandelion's umbrella-shaped structure on its drag force and attitude stability. The numerical simulation results have shown that as the folding angle increases, the drag coefficient of the dandelion gradually decreases, but the restoring moment under side wind disturbance gradually rises. This indicates that dandelion needs to maintain an appropriate folding angle to achieve a balance between high drag force and good attitude stability. The proposed model suggested that when the folding angle is approximately between 20° and 40°, the dandelion seeds may have a good balance between drag force and attitude stability, which accommodates a broad self-adapted flying ability for the seeds.

This study is able to shed some light on the dandelion flying mechanism, and the findings of the study can also provide instructions for the design of dandelion-inspired unpowered aircraft.

17 August 2023 11:44:26

AUTHOR DECLARATIONS
Conflict of Interest

The authors have no conflicts to disclose.

Author Contributions

Lang Qin: Formal analysis (lead); Methodology (lead); Writing – original draft (lead); Writing – review & editing (equal). **Zhen Jian:** Formal analysis (equal); Funding acquisition (equal); Supervision (equal); Writing – review & editing (equal). **Yeyin Xu:** Resources (equal); Software (equal). **Lifeng Ma:** Funding acquisition (supporting); Resources (equal); Supervision (equal); Writing – review & editing (equal).

DATA AVAILABILITY

The data that support the findings of this study are available from the corresponding authors upon reasonable request.

REFERENCES

[1] H. F. Howe and J. Smallwood, "Ecology of seed dispersal," Annu. Rev. Ecol. Syst. **13**, 201–228 (1982).

[2] R. Nathan, F. M. Schurr, O. Spiegel, O. Steinitz, A. Trakhtenbrot, and A. Tsoar, "Mechanisms of long-distance seed dispersal," Trends Ecol. Evol. **23**, 638–647 (2008).

[3] J. Sirohi, "Microflyers: Inspiration from nature," Bioinspiration, Biomimetics, Bioreplication **8686**, 134–148 (2013).

[4] B. H. Kim, K. Li, J.-T. Kim, Y. Park, H. Jang, X. Wang, Z. Xie, S. M. Won, H.-J. Yoon, and G. Lee, "Three-dimensional electronic microfliers inspired by wind-dispersed seeds," Nature **597**, 503–510 (2021).

[5] E. Barta and D. Weihs, "Creeping flow around a finite row of slender bodies in close proximity," J. Fluid Mech. **551**, 1–17 (2006).

[6] G. Davidi and D. Weihs, "Flow around a comb wing in low-Reynolds-number flow," AIAA J. **50**, 249–253 (2012).

[7] J. Sundin and S. Bagheri, "Interaction between hairy surfaces and turbulence for different surface time scales," J. Fluid Mech. **861**, 556–584 (2019).

[8] M. C. Andersen, "Diaspore morphology and seed dispersal in several wind-dispersed Asteraceae," Am. J. Bot. **80**, 487–492 (1993).

[9] I. Hensen and C. Müller, "Experimental and structural investigations of anemochorous dispersal," Plant Ecol. **133**, 169–180 (1997).

[10] M. B. Soons and J. M. Bullock, "Non-random seed abscission, long-distance wind dispersal and plant migration rates," J. Ecol. **96**, 581 (2008).

[11] C. Cummins, M. Seale, A. Macente, D. Certini, E. Mastropaolo, I. M. Viola, and N. Nakayama, "A separated vortex ring underlies the flight of the dandelion," Nature **562**, 414–418 (2018).

[12] E. Zussman, A. Yarin, and D. Weihs, "A micro-aerodynamic decelerator based on permeable surfaces of nanofiber mats," Exp. Fluids **33**, 315–320 (2002).

[13] Q. Meng, Q. Wang, K. Zhao, P. Wang, and J. Lei, "Hydroactuated configuration alteration of fibrous dandelion pappi: Toward self-controllable transport behavior," Adv. Funct. Mater. **26**, 7378 (2016).

[14] M. Seale, A. Kiss, S. Bovio, I. M. Viola, E. Mastropaolo, A. Boudaoud, and N. Nakayama, "Dandelion pappus morphing is actuated by radially patterned material swelling," Nat. Commun. **13**, 2498 (2022).

[15] M. Seale, O. Zhdanov, M. B. Soons, C. Cummins, E. Kroll, M. R. Blatt, H. Zare-Behtash, A. Busse, E. Mastropaolo, and J. M. Bullock, "Environmental morphing enables informed dispersal of the dandelion diaspore," Elife **11**, e81962 (2022).

[16] F.-S. Qiu, T.-B. He, and W.-Y. Bao, "Effect of porosity on separated vortex rings of dandelion seeds," Phys. Fluids **32**, 113104 (2020).

[17] F.-S. Qiu, B.-W. Wang, Y.-M. Du, and H.-Y. Qian, "Numerical investigation on the flow characteristics of model dandelion seeds with angles of attitude," Phys. Fluids **33**, 113107 (2021).

[18] F.-S. Qiu, H.-Y. Qian, Y.-M. Du, and C.-J. Li, "The pappus angle as a key factor in the entire separation of a vortex ring from a dandelion seed's pappus," Phys. Fluids **34**, 083101 (2022).

[19] Y. Dong, K. Hu, Y. Wang, and Z. Zhang, "The steady vortex and enhanced drag effects of dandelion seeds immersed in low-Reynolds-number flow," AIP Adv. **11**, 085320 (2021).

[20] S. Li, D. Pan, J. Li, and X. Shao, "Drag and wake structure of a quasi-dandelion pappus model at low and moderate Reynolds numbers: The effects of filament width," Phys. Fluids **33**, 121904 (2021).

[21] V. Casseau, G. De Croon, D. Izzo, and C. Pandolfi, "Morphologic and aerodynamic considerations regarding the plumed seeds of Tragopogon pratensis and their implications for seed dispersal," PLoS ONE **10**, e0125040 (2015).

[22] M. Ciuti, G. Zampogna, F. Gallaire, S. Camarri, and P. Ledda, "On the effect of a penetrating recirculation region on the bifurcations of the flow past a permeable sphere," Phys. Fluids **33**, 124103 (2021).

[23] C. Cummins, I. M. Viola, E. Mastropaolo, and N. Nakayama, "The effect of permeability on the flow past permeable disks at low Reynolds numbers," Phys. Fluids **29**, 097103 (2017).

[24] P. G. Ledda, L. Siconolfi, F. Viola, F. Gallaire, and S. Camarri, "Suppression of von Kármán vortex streets past porous rectangular cylinders," Phys. Rev. Fluids **3**, 103901 (2018).

[25] T. Tang, J. Xie, S. Yu, J. Li, and P. Yu, "Effect of aspect ratio on flow through and around a porous disk," Phys. Rev. Fluids **6**, 074101 (2021).

[26] L. Zong and H. Nepf, "Vortex development behind a finite porous obstruction in a channel," J. Fluid Mech. **691**, 368–391 (2012).

[27] M. Liu, C. Xie, M. Yao, and J. Yang, "Study on the near wake of a honeycomb disk," Exp. Therm Fluid Sci. **81**, 33–42 (2017).

[28] K. Steiros, K. Kokmanian, N. Bempedelis, and M. Hultmark, "The effect of porosity on the drag of cylinders," J. Fluid Mech. **901**, R2 (2020).

[29] P. G. Ledda, L. Siconolfi, F. Viola, S. Camarri, and F. Gallaire, "Flow dynamics of a dandelion pappus: A linear stability approach," Phys. Rev. Fluids **4**, 071901 (2019).

[30] P. G. Ledda, E. Boujo, S. Camarri, F. Gallaire, and G. Zampogna, "Homogenization-based design of microstructured membranes: Wake flows past permeable shells," J. Fluid Mech. **927**, A31 (2021).

[31] D. Fabre, P. Assemat, and J. Magnaudet, "A quasi-static approach to the stability of the path of heavy bodies falling within a viscous fluid," J. Fluids Struct. **27**, 758–767 (2011).

[32] J. Tchoufag, J. Magnaudet, and D. Fabre, "Linear instability of the path of a freely rising spheroidal bubble," J. Fluid Mech. **751**, R4 (2014).

[33] D. Sujudi and R. Haimes, "Identification of swirling flow in 3-D vector fields," in the 12th Computational Fluid Dynamics Conference, San Diego, CA (AIAA, 1995).

17 August 2023 11:44:26